Mechanism and Machine Theory 50 (2012) 90–108

Contents lists available at SciVerse ScienceDirect

Mechanism and Machine Theory

journal homepage: www.elsevier.com/locate/mechmt

Optimal design and kinetic analysis of a stair-climbing mobile robot with rocker-bogie mechanism

Dongmok Kim [a], Heeseung Hong [a], Hwa Soo Kim [b,*], Jongwon Kim [a]

[a] School of Mechanical and Aerospace Engineering, Seoul National University, 599 Gwanak-ro, Gwanak-gu, Seoul 151-742, Republic of Korea
[b] Department of Mechanical System Engineering, Kyonggi University, San 94-6, Iui-dong, Yeongtong-gu, Kyonggi-do 443-760, Republic of Korea

ARTICLE INFO

Article history:
Received 21 April 2011
Received in revised form 15 November 2011
Accepted 22 November 2011
Available online 23 December 2011

Keywords:
Wheel-type mobile robot
Rocker-bogie mechanism
Taguchi method
Friction requirement metric
Kinetic analysis

ABSTRACT

Based on the well-known rocker-bogie mechanism, this paper first presents an optimal design of a wheel-type mobile robot in order to ensure high mobile stability as well as excellent adaptability while climbing stairs. As an optimization tool, the Taguchi method is adopted due to its simplicity and cost-effectiveness both in formulating an objective function and in satisfying multiple constraints simultaneously. The sensitivity analysis with respect to design parameters is carried out to provide an insight to their effects on the performance criterion under kinematic constraints which are imposed to avoid undesired interferences between a mobile robot and stairs. To evaluate the climbing capability of the optimized rocker-bogie mechanism, the friction requirement metric is chosen, which is defined as a minimum friction coefficient required for a mobile robot to climb a stair without slip. Through a kinetic analysis of a stair-climbing motion, a locomotive strategy suitable for the proposed rocker-bogie mechanism is derived to minimize slip while climbing a stair and successfully verified through extensive simulations.

1. Introduction

Over the last decade, mobile robots have been widely used to carry out manifold tasks such as military/industrial applications [1–4], planetary exploration [5–8], rescue operation [9,10] and home/medical services [11,12]. Therefore, it is not surprising that high mobility on various environments has been a primary factor among others when evaluating the performance of the mobile robot [13].

According to a locomotive mechanism to achieve the desired mobility, mobile robots may be split into following categories: leg-type, track-type and wheel-type mobile robots. While the leg-type mobile robot ensures the most superior adaptability to all kinds of environments, its mechanism is quite complicated because active control algorithms equipped with additional actuators and sensors are required to steadily maintain its balance, which inevitably leads to slow movement and poor energy efficiency [14,15]. The track-type mobile robot provides acceptable mobility on an off-road environment by virtue of its inherently stable mechanism but excessive friction loss during changing a direction also results in poor energy efficiency [16]. Compared to other alternatives, the wheel-type mobile robot can be constructed in the simplest configuration so that fast movement as well as good energy efficiency are guaranteed without any complicated control strategy. However, its adaptability to an environment does not seem to be sufficiently good and its mobility is restricted depending on both the type and the size of encountered obstacle [15,17].

Recently, hybrid-type mobile robots have been suggested in various configurations by combining two locomotive mechanisms together [13,18,19]. However, their mechanisms still seem to be complicated in comparison with the wheel-type one and from the viewpoint of control, the cooperation between locomotion mechanisms emerges as another important issue [17]. On the

* Corresponding author. Tel.: +82 31 249 9806; fax: +82 31 244 6300.
E-mail address: hskim94@kgu.ac.kr (H.S. Kim).

0094-114X/$ – see front matter © 2011 Elsevier Ltd. All rights reserved.
doi:10.1016/j.mechmachtheory.2011.11.013

other hand, several wheel-type locomotive mechanisms equipped with passive linkages have successfully verified their mobile performances in real applications, for example, Mars Exploration Rovers (MERs) like Sojourner, Rocky7, Spirit and Opportunity [5–7], ORF-L [8], CEDRA [9], SHRIMP [16], etc. Among those passive linkages, the rocker-bogie is well known, which consists of two structural elements called as "rocker" and "bogie". A schematic diagram of a six-wheeled rocker-bogie mechanism and the real photograph of Spirit adopting this mechanism are shown in Fig. 1(a) and (b), respectively. The two-wheeled bogie is connected to the rocker through a pivot and two rockers on both sides are coupled to each other via a differential joint. Since all wheels of the rocker-bogie mechanism can keep in contact with the ground under various environments, it is possible not only to equilibrate the pressure of each wheel on the ground but also to effectively move forward/backward. Also, this mechanism allows a mobile robot to maintain its balance at the average pitch angle of both rockers so that the possibility of tip-over can be reduced [20,21].

In order to improve the climbing capability of a wheel-type mobile robot specially against structured terrains such as steps and stairs, several mechanisms have been developed on the basis of the rocker-bogie so that a few mobile robots can climb even steps of twice their wheel diameter [9,16,22]. However, they often suffer from undesired phenomenon that some wheels float from the ground while climbing steps and stairs [22,23], which may cause instability of the mobile robot. It is worthwhile to note that a trajectory of center of mass (CM) may serve as a tool for effectively predicting such undesirable phenomenon which is likely to occur at the moment the trajectory of CM drastically or discontinuously changes. Therefore, it is highly required to make the trajectory of CM as smooth as possible, which implies that the trajectory of CM must be close to a straight line whose slope is determined by a step or a stair. Since this requirement on the trajectory of CM minimizes the required motor power, the possibility is increased that the mobile robot can efficiently climb a step or a stair even for the relatively low friction coefficient [9,16].

Based on the rocker-bogie mechanism, an optimal design of a stair-climbing wheel-type mobile robot is first presented. The Taguchi method is chosen as an optimization tool to make the trajectory of CM close to the straight line while all wheels keep in contact with the ground during climbing stairs. The optimization procedure is carried out against various sizes of stairs, which will significantly improve the robustness as well as the adaptability to structured terrains frequently encountered in indoor applications. Then, in order to fully exploit the behavior of the proposed rocker-bogie mechanism during climbing the stair, its corresponding motions are divided into several phases that show the status of the interaction between the wheels and the

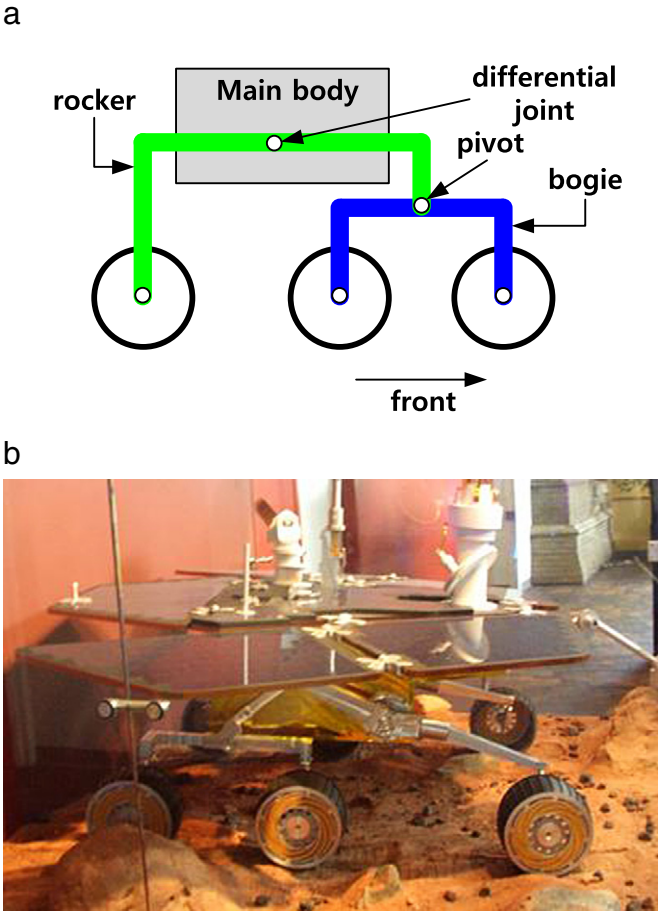

Fig. 1. (a) Schematic diagram of rocker-bogie mechanism and (b) real photograph of Spirit.

stair. Using the simplified mathematical model for the proposed rocker-bogie mechanism, a kinetic analysis is performed to derive the most suitable locomotive strategy for each phase, which enables the proposed mechanism to efficiently climb the stair combined with the kinematic optimization result. The effectiveness of proposed locomotive strategy is subsequently examined through the extensive simulations against different sizes of stairs.

The rest of this paper is organized as follows. In Section 2, the kinematic constraints on the rocker-bogie mechanism are derived to prevent undesired interferences among a stair, its wheels and links during climbing a stair. Based on these constraints in Section 2, the optimization procedure via the Taguchi method is presented and the obtained optimal design is compared with others in Section 3. Section 4 suggests a locomotive strategy suitable to the proposed rocker-bogie mechanism through the kinetic analysis and validates its effectiveness against various sizes of stairs.

2. Kinematic constraints on the rocker-bogie mechanism

It is worthwhile to consider kinematic constraints on the rocker-bogie mechanism so as to prevent undesired interferences among a stair, its wheels and links. For the simplicity of optimization procedure, a 2-D model for the rocker-bogie mechanism is chosen similar to the ones in [16,24]. As shown in Fig. 2, its CM is assumed to be located exactly above the joint *A* connecting two *Link* 1 and *Link* 2 and then, three wheel radii (R_1, R_2 and R_3) and four link lengths (l_1, l_2, l_3 and l_4) are selected as design parameters.

Since various sizes of stairs may be encountered in real applications, three types of stairs are considered to derive the kinematic constraints on the rocker-bogie mechanism, whose tread and riser lengths are 300 mm × 100 mm, 310 mm × 160 mm and 240 mm × 200 mm and the corresponding slopes are 18.4°, 27.3° and 39.8°, respectively. The detailed configurations of three stairs are shown in Fig. 3.

First, the minimum wheel radius is determined to be 25 mm (about 1 in.) considering the smallest size of wheel commercially obtainable. The kinematic constraint on the maximum wheel radius is described through Fig. 4 where before climbing the upper step of stair, a wheel center can stay on the tread of stair in order to steadily maintain its posture. Therefore, these constraints on the wheel radius R_i, i = 1, 2, 3 can be expressed by

$$25 \text{ mm} \le R_i \le 244 \text{ mm}. \tag{1}$$

Next, each link length l_i should be greater than the wheel radius R_i, i = 1, 2, 3 because undesired interferences between the wheels themselves may occur if not so. Assuming that the overall size of the rocker-bogie mechanism in this study is smaller than 1 m^3, the maximum link length is bounded by 1 m, which is simply given by

$$R_i < l_i \le 1000 \text{ mm}. \tag{2}$$

In addition, since two wheels W_1 and W_2 of the bogie mechanism are connected through the *Link* 1, the link length l_4 should be greater than $R_1 + R_2$ to avoid the interference between those wheels as described in Fig. 5(a). Similarly, another condition may be derived in order to avoid the interference between two wheels W_2 and W_3 as shown in Fig. 5(b). Combined with a geometric condition that the *Link* 1 is in the shape of a triangle, the above constraints are summarized by

$$\begin{cases} l_4 > R_1 + R_2 \\ l_3 - R_3 > l_2 + R_2 \\ l_1 + l_2 \ge l_4, \quad l_2 + l_4 \ge l_1, \quad l_4 + l_1 \ge l_2 \end{cases}. \tag{3}$$

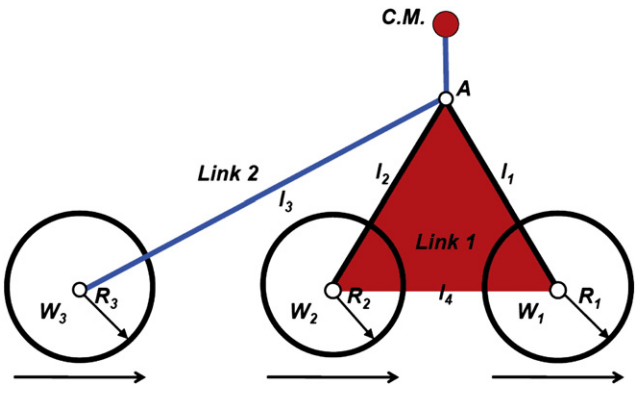

Fig. 2. Schematic diagram of 2-D model for the rocker-bogie mechanism.

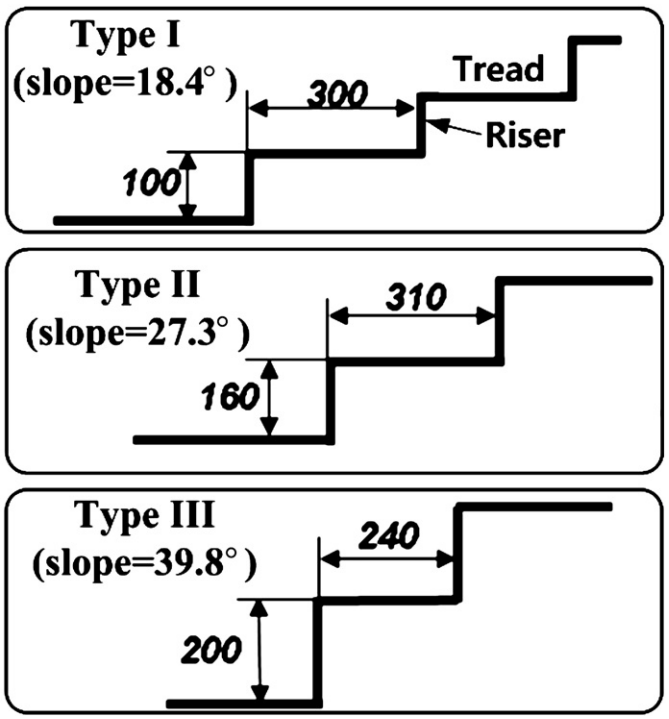

Fig. 3. Three types of stairs.

Due to the kinematic characteristics of the bogie mechanism that two wheels are connected by the *Link* 1, at least one between two wheels should stay on the tread of stair in order to prevent the rocker-bogie mechanism from getting stuck during climbing the stair [23]. If both wheels of the bogie mechanism move up along the riser of stair, the rocker-bogie mechanism does not seem to succeed in climbing the stair because only the rear wheel W_3 supports the whole mechanism. Therefore, as shown in Fig. 6, it is highly desired that W_2 is on the tread of stair until W_1 completes climbing the riser of stair or W_1 is on the tread of stair until W_2 completes climbing the riser of stair. In combination with a safety margin of 10% to the tread length of stair, this kinematic constraint on the link length l_4 and two wheels' radii R_1 and R_2 is expressed as

$$\sqrt{(R_2+0.1a)^2+(b+R_1-R_2)^2} \le l_4 \le \sqrt{(0.9a-R_1)^2+(R_1-R_2)^2}. \tag{4}$$

Finally, the joint A should be far away from the edge of stair so as not to interfere with the stair as shown in Fig. 7(a). Therefore, when the joint A comes close to the vertical line $\overline{B_1B_2}$, it should be above the horizontal line $\overline{C_1C_2}$ as shown in Fig. 7(b). Assuming

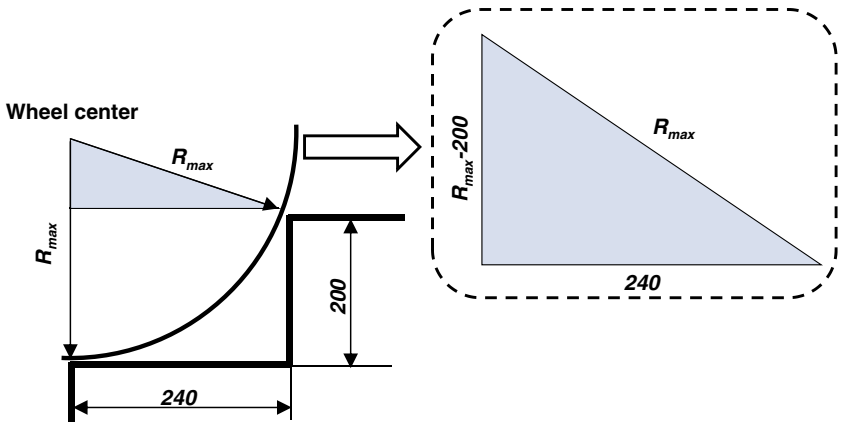

Fig. 4. Constraint on maximum wheel radius.

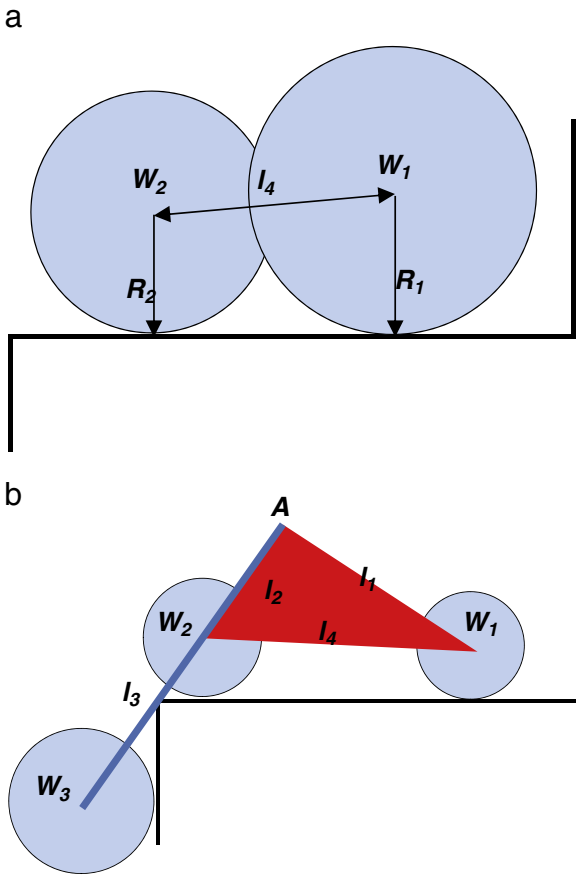

Fig. 5. Interferences (a) between two wheels W_1 and W_2 of the bogie mechanism and (b) between two wheels W_2 and W_3.

that a distance between the joint A and the stair is at least greater than 15 mm, this constraint is expressed with the safety margin of 10% to the minimum distance as

$$\left(\sqrt{{l_4}^2-t^2}\sin\delta + t\cos\delta\right)\frac{l_2}{l_4} + R_1 - t \geq 1.1 \times 15 \ \text{mm} \tag{5}$$

where the angle δ between l_2 and l_4 is given by $\delta = \cos^{-1}\left(\frac{{l_2}^2+{l_4}^2-{l_1}^2}{2l_2l_4}\right)$ and $t = \frac{l_4}{l_2\sin\delta}[\{(R_2-15)\cos\delta + \sqrt{\left({l_2}^2-(R_2-15)^2\right)\sin^2\delta}\}\cos\delta-(R_2-15)]$. Recall that the additional safety margin of 10% is included specially in Eqs. (4) and (5) to ensure the robustness of the optimized parameters against various sizes of stairs encountered in real applications.

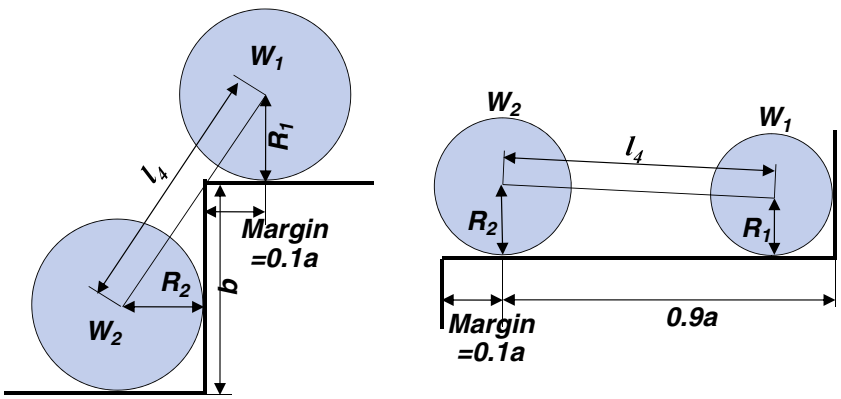

Fig. 6. Ideal movements of two wheels W_1 and W_2.

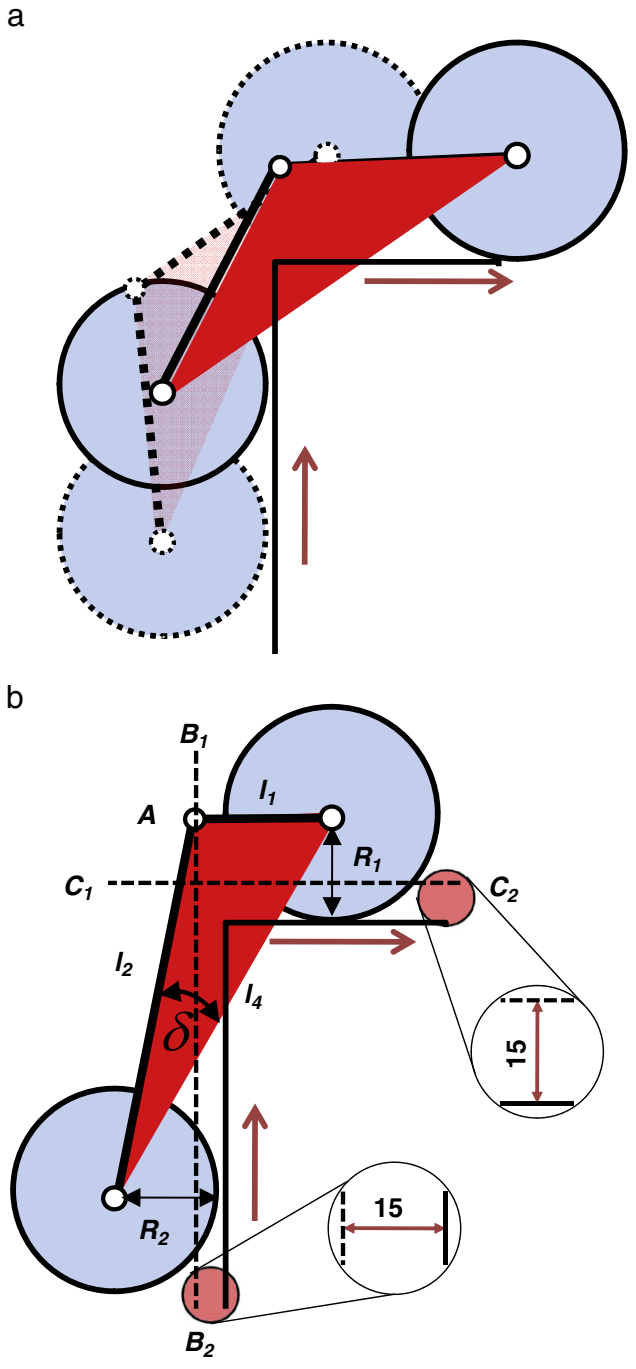

Fig. 7. (a) Ideal movement of joint *A* and (b) corresponding constraint on the position of joint *A*.

3. Optimization procedure via Taguchi method

3.1. Objective function

Under the kinematic constraints in Eqs. (1)–(5), the optimization is subsequently carried out in this section. As previously discussed in Section 1, the objective of optimization is to make the trajectory of CM close to a straight line. Since the slope of the stair may vary according to its size, it does not seem reasonable to fix the slope of straight line. Therefore, the goal of this optimization is refined to minimize an area between the trajectory of CM and the straight line whose slope is equal to that of the stair. Since all portions of CM trajectory are equally handled in the proposed objective function, it seems much suitable for the rocker-bogie

based wheel-type mobile robot which moves backward when starting to climb a stair in comparison with [9] where some portions of CM trajectory that have a positive slope are considered (more detailed discussion will be given in Section 3.3). The exemplary illustration of the objective function is given in Fig. 8, where the trajectory of CM, the straight line and the corresponding area between them are denoted by the blue line of rectangular mark, the red line and the dotted blue line, respectively and the origin of straight line is determined to be a position of CM at the moment the front wheel W_1 keeps contact with the riser of the stair.

Recall that the CM defined in the paper corresponds to that of the mobile robot body including the payloads except links and wheels. Since the CM position of the mobile robot may change according to its posture during climbing a stair, an electrical cylinder will be added to maintain its CM position horizontally despite its posture during a stair, which connects the *Link* 2 with the robot body. Therefore, without loss of generality, the CM of the mobile robot is assumed to be fixed in this paper so that during climbing a stair, its trajectory can be obtained from the kinematic relation between the wheels and the links. It is also worthwhile to note that for each simulation step, the mobile robot moves forward a short, well-defined distance along the stair so that the trajectory of each wheel center is naturally determined for given wheels and link parameters. The following steps summarize how the CM trajectory of the proposed rocker-bogie mechanism is calculated.

S1. For the given position of the front wheel center, the corresponding position of the middle wheel center is determined as a point on its trajectory whose distance from the front wheel center is l_4.
S2. Then, the position of the joint A can be determined by the geometric condition that the *Link* 1 is in the shape of a triangle.
S3. Similar to S1, the position of the rear wheel is determined as a point on the trajectory of the rear wheel center whose distance from the joint A is l_3. Subsequently, the angle θ_2 between the *Link* 2 and the horizontal axis is calculated by using Eqs. (11) and (12).
S4. Finally, the position of CM can be determined by rotating the link whose length is Δ through θ_2 around the joint A. These steps are repeated to obtain the successive CM trajectory.

3.2. Taguchi method

The Taguchi method is a systematic design approach to find an optimal value of each parameter by design of experiments or simulations [25–28]. Compared to the theoretical optimization approaches which generally demand complicated mathematical expansions, it is quite simple and cost-effective not only in formulating the objective function but also in satisfying the multiple quality requirements simultaneously. In this method, all primary factors that affect the performance measure such as signal-to-noise (S/N) ratio may be classified into two categories: control and noise factors. Since the control factors can be chosen by a designer, they are easily adjustable to have desired values but the noise factors are difficult to control so that they may cause variations or detrimental effects to the product quality [26]. Therefore, such parameters as the wheel radii (R_1, R_2 and R_3) and the link lengths (l_1, l_2, l_3 and l_4) are selected as control factors and three stairs in Fig. 3 are selected as noise factors, respectively.

3.2.1. S/N ratio

As the performance measure to evaluate the quality of chosen link parameters in the presence of noise factors, the S/N ratio is introduced in the Taguchi method [25]. The principal goal of the optimization is to maximize the S/N ratio because the S/N ratio becomes higher, the effect of random noise factors on the performance can be reduced. It is worthwhile to note that the objective of this optimization is to minimize the area between the trajectory of CM and the straight line determined by each stair so that

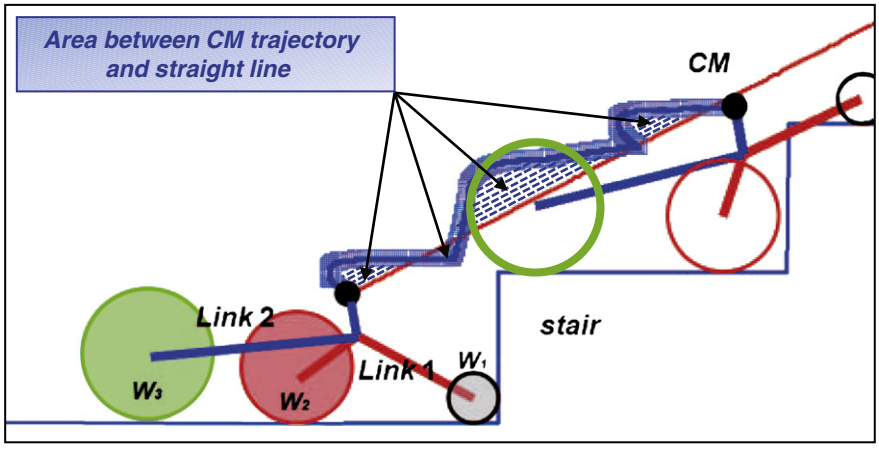

Fig. 8. Illustration of objective function.

Table 1
Levels of control factors and initial values for the 1st simulation.

Control factor	Level 1 (mm)	Level 2 (mm)	Level 3 (mm)
R_1	25	35	–
l_1	180	190	200
l_2	70	80	90
l_3	210	220	230
l_4	180	190	200
R_2	60	70	80
R_3	60	70	80

this optimization corresponds to the-smaller-the-better case. Therefore, among various types of S/N ratios, the following one is selected considering the objective of this optimization.

$$S/N = -10\ \log_{10}\left\{\frac{1}{N}\sum_{i=1}^{N} y_i^2\right\}[\mathrm{dB}] \tag{6}$$

where N is the number of repetitions in simulations and y_i is the performance value of the ith simulation. In this study, since the optimization is carried out with respect to three types of stairs in Fig. 3, N is equal to the number of stairs and y_i denotes the area between the trajectory of CM and the straight line determined by the ith stair. It is noted that to maximize S/N ratio in Eq. (6) is equivalent not only to minimize each area y_i, $i=1, 2, 3$, but also to minimize the variation between them since the selected S/N ratio in this study can be rephrased as follows:

$$\begin{aligned} S/N &= -10\ \log_{10}\left\{\frac{y_1^2+y_2^2+y_3^2}{3}\right\} \\ &= -10\ \log_{10}\left\{\frac{(y_1+y_2+y_3)^2+(y_1-y_2)^2+(y_2-y_3)^2+(y_3-y_1)^2}{3}\right\}. \end{aligned}$$

3.2.2. Design of simulations using orthogonal arrays

In order to streamline the optimization procedure via the Taguchi method, the preliminary study is performed to obtain the area between the trajectory of CM calculated from the predetermined design parameters of rocker-bogie mechanism and the straight line for three stairs in Fig. 3, which shows that the front wheel radius R_1 is bounded by the upper limit in Eq. (1). Since it implies that an S/N ratio in Eq. (6) increases as R_1 becomes smaller, a level of control factor R_1 is chosen to be 2 while levels of others are set to 3 so as to capture a clue to their trends toward the optimal values. The levels of control factors and their initial values are shown in Table 1.

Table 2
Resulting objective functions and S/N ratios in the 1st simulation.

No.	Control factors								Objective function			S/N [dB]
	R_1	l_1	l_2	l_3	l_4	R_2	R_3	–	y_1	y_2	y_3	
1	1	1	1	1	1	1	1	1	6882	12,957	15,076	−81.69
2	1	1	2	2	2	2	2	2	6900	13,132	13,113	−81.16
3	1	1	3	3	3	3	3	3	7552	14,961	13,468	−81.88
4	1	2	1	1	2	2	3	3	6733	12,756	13,874	−81.26
5	1	2	2	2	3	3	1	1	6890	13,563	14,161	−81.58
6	1	2	3	3	1	1	2	2	7286	14,036	14,720	−81.92
7	1	3	1	2	1	3	2	3	7678	15,114	17,310	−82.92
8	1	3	2	3	2	1	3	1	7159	13,371	14,228	−81.59
9	1	3	3	1	3	2	1	2	6691	13,324	14,327	−81.54
10	2	1	1	3	3	2	2	1	5951	10,739	11,124	−79.61
11	2	1	2	1	1	3	3	2	6957	14,056	14,769	−81.89
12	2	1	3	2	2	1	1	3	6241	11,858	12,801	−80.59
13	2	2	1	2	3	1	3	2	6541	11,454	13,666	−80.80
14	2	2	2	3	1	2	1	3	7033	13,761	15,266	−81.97
15	2	2	3	1	2	3	2	1	6730	13,890	14,850	−81.84
16	2	3	1	3	2	3	1	2	6887	13,348	15,082	−81.79
17	2	3	2	1	3	1	2	3	6836	12,382	15,200	−81.57
18	2	3	3	2	1	2	3	1	7267	14,622	16,151	−82.45

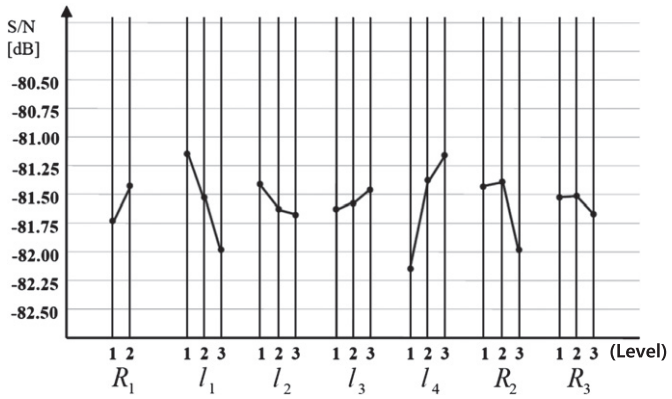

Fig. 9. Average *S/N* ratios with respect to control factors in the 1st simulation.

For given control and noise factors, a design of full factorial simulations is required to investigate their effects on the quality requirement simultaneously. However, since the total number of simulations from all possible combinations of these factors is up to 4374 ($=3\times2\times3^6$), it seems quite iterative and time-consuming to carry out full factorial simulations. In order to tactfully handle this difficulty, an orthogonal array is adopted in the Taguchi method, which enables to efficiently find out some critical factors affecting the product quality even with a minimum number of simulations. Considering the number of noise/control factors and their levels, the orthogonal array $L_{18}(2\times3^7)$ is first selected so that the total number of required simulations can be significantly reduced to 54 [28].

3.3. Simulation results

The task of optimizing the link parameters of rocker-bogie mechanism via the Taguchi method starts from the sensitivity analysis based on *S/N* ratio, which helps to figure out critical control factors to play key roles in determining the objective function in Section 3.1. Focusing on these meaningful control factors, the optimization procedures are subsequently repeated to search for optimal values by appropriately adopting another reduced orthogonal array.

For each simulation from the orthogonal array L_{18}, the resulting objective function y_i, $i=1, 2, 3$, and the *S/N* ratio are summarized in Table 2. In order to unravel the underlying effects of various control factors on the objective function, the average *S/N* ratios are calculated for each control factor at different levels as shown in Fig. 9. For the simplicity of notation, the level of control factor is represented by a superscript, for example, R_1^2 implies the control factor R_1 of the level 2. It is observed from Fig. 9 that R_1^2, l_1^1, l_2^1, l_3^3, l_4^3, R_2^2, R_3^2 are optimal because corresponding average *S/N* ratio is maximized at those levels of control factors, which is also confirmed in Table 2 showing that the maximum of *S/N* ratio ($=-79.61$ dB) occurs at the same combination of control factors.

It should be noted that the kinematic constraints in Section 2 are not reflected in the initial values of control factors because it is impossible to predict a combination of optimal control factors satisfying those constraints. For such a combination of control factors as (R_1^2, l_1^1, l_2^1, l_3^3, l_4^3, R_2^2, R_3^2), two constraints in Eqs. (1) and (4) are violated so that the undesired interference between the wheel W_2 and the joint A may occur and both wheels W_1 and W_2 of bogie mechanism may stay along the riser of stair simultaneously.

The first problem related with Eq. (1) can be attacked by simply increasing the level of l_2 or decreasing the level of R_2. Since the average *S/N* ratio at R_2 of the level 1 is larger than that at l_2 of the level 2 as shown in Fig. 9, the optimal level of R_2 is adjusted from 2 to 1. Similarly, the levels of R_1 and l_4 are reduced to 1 and 2, respectively in order to satisfy the kinematic constraint in Eq. (4) combined with R_2^1. As a result, the *S/N* ratio is slightly deteriorated from $_?-79.61$ dB to $_?-80.38$ dB for a modified combination of control factors like (R_1^1, l_1^1, l_2^1, l_3^3, l_4^2,R_2^1, R_3^2). However, please note that it is still higher than those obtained from other combinations of control factors.

It is worthwhile to note from Fig. 9 that in comparison with other control factors, three control factors l_1, l_4 and R_2 have strong effects on the average *S/N* ratios due to their high sensitivities. Based on this observation, the additional simulation focusing on these control factors l_1, l_4 and R_2 is subsequently performed with the orthogonal array $L_9(3^4)$ as shown in Table 3. While smaller values are chosen for the levels of l_1 in the second simulation because its optimal level in the first simulation is 1, the levels of l_4

Table 3
Levels of reduced control factors and initial values for the 2nd simulation.

Control factor	Level 1 (mm)	Level 2 (mm)	Level 3 (mm)
l_1	170	175	180
l_4	185	190	195
R_2	55	60	65

Table 4
Resulting objective functions and *S/N* ratios in 2nd simulation.

No.	Control factors				Objective function			*S/N* [dB]
	l_1	l_4	R_2	–	y_1	y_2	y_3	
1	1	1	1	1	6473	11,505	11,607	−80.13
2	1	2	2	2	6359	11,307	10,982	−79.84
3	1	3	3	3	6294	11,267	10,547	−79.67
4	2	1	2	3	6639	12,011	11,935	−80.42
5	2	2	3	1	6531	11,846	11,362	−80.17
6	2	3	1	2	6267	10,851	11,477	−79.83
7	3	1	3	2	6808	12,537	12,361	−80.75
8	3	2	1	3	6566	11,673	12,464	−80.48
9	3	3	2	1	6389	11,302	11,677	−80.07

and R_2 in the first simulation are set to medium levels in the second simulation considering that their trends toward the optimal values still remain unknown.

For each simulation from the orthogonal array L_9, the resulting objective function y_i, $i = 1, 2, 3$, and the *S/N* ratios in the second simulation are summarized in Table 4.

Recall that optimal values of other control factors except l_1, l_4 and R_2 are already determined in the first simulation. The average *S/N* ratios are calculated for l_1, l_4 and R_2 at different levels and compared to those in the first simulation denoted by gray lines in Fig. 10.

According to the second simulation, the optimal levels for l_1, l_4 and R_2 are 1, 3 and 2, respectively and the corresponding *S/N* ratios are significantly improved more than by 1.5 dB in comparison with those in the first simulation. As for the control factor R_2, the difference between minimum and maximum average *S/N* ratios is less than 0.1 dB so that its optimal value is determined to be 70 mm. It is again checked whether the kinematic constraints in Eqs. (1)–(5) are satisfied with the combination of (l_1^1, l_4^3, R_2^1) plus $(R_1^1, l_2^1, l_3^3, R_3^2)$. However, since the constraint in Eq. (4) is not satisfied with this combination of control factors, the level of l_4 related with this constraint is adjusted from 3 to 2 and as a result, the *S/N* ratio is slightly shifted from −79.53 dB to −79.84 dB but is still larger than that (= −80.38 dB) in the first simulation.

As for l_1 and l_4 still suffering from high sensitivity, additional simulations are carried out twice in the similar manner with the orthogonal array L_9. Of course, the resulting optimal values of those two control factors are guaranteed to satisfy the kinematic constraints in Eqs. (1)–(5). It is noted that although the number of control factors to be optimized in additional simulations is reduced to 2, the orthogonal array L_9 is still used because it is of the smallest size among orthogonal arrays available to represent two control factors of three levels.

Table 5 summarizes the optimal values of control factors for the rocker-bogie mechanism. In order to make the trajectory of CM close to the straight line, the wheel radii of the optimized rocker-bogie mechanism naturally become smaller along a moving direction as shown in Fig. 11. Also, since the angle between l_2 and l_4 is larger than that between l_1 and l_4 as confirmed in Fig. 11, the proposed rocker-bogie mechanism is likely to turn counter-clockwise, which helps to passively climb up a stair. However, since the center of the front wheel W_1 is located below that of the middle wheel W_2, supplementary moments may be required to lift W_1 up along the riser of the stair so that a suitable locomotive strategy for the proposed rocker-bogie mechanism should be developed, which will be in detail discussed in Section 4.

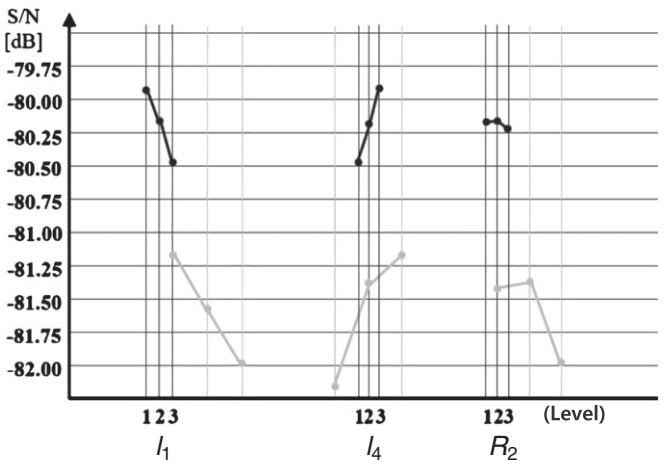

Fig. 10. Average *S/N* ratios with respect to three control factors in the 2nd simulation.

Table 5
Optimal values of control factors for the rocker-bogie mechanism.

l_1	l_2	l_3	l_4	R_1	R_2	R_3
140	70	230	194	25	60	70

3.4. Discussion

In order to evaluate the performance of the optimized rocker-bogie mechanism, the general rocker-bogie and the Mars rover Spirit in Fig. 1(b) are considered together. The parameter values of the general rocker-bogie mechanism are taken from the worst combination of control factors in Table 1 and those of the Mars rover Spirit are appropriately scaled from [29] for a fair comparison. As a criterion for scaling down, the wheel size is chosen so that its wheel diameter is reduced from 200 mm to 120 mm, which is equal to that of the middle wheel W_2 of the optimized rocker-bogie mechanism. Other parameter values in [29] are scaled down in the same ratio of 5 to 3.

For three stairs in Fig. 3, Fig. 12 compares the CM trajectory of the optimized rocker-bogie mechanism with those of the general rocker-bogie and the scaled-down Mars rover Spirit. The dashed, blue solid and dash–dotted lines in Fig. 12 represent the CM trajectories of the scaled-down Mars rover Spirit and the optimized/general rocker-bogie mechanisms, respectively and the slope of each stair is denoted by the straight dotted line. For each stair, the error between the trajectory of CM and the straight line is computed while climbing one step. As shown in Fig. 12, those errors are considerably reduced for the optimized rocker-bogie mechanism compared to others and as the stair becomes much steeper, the differences among those errors increase more than by 21%, which implies that the CM trajectory of the optimized rocker-bogie mechanism is nearest to various straight lines regardless of their slopes. Even though it is observed in Fig. 12 that all trajectories of CM initially move backward and then continue forward as pointed out in [9], the backward distance of the optimized rocker-bogie mechanism becomes much shorter than those of the scaled-down Mars rover Spirit and the general rocker-bogie, which enables the proposed rocker-bogie mechanism to climb the stair more efficiently and rapidly. Due to this initial backward movement of the rocker-bogie mechanism before climbing the stair, the objective function selected in [9] which considers only the CM trajectories of positive slope does not seem to be suitable for the optimization of the rocker-bogie mechanism because the slope of the CM trajectory becomes infinite when its slope changes from negative to positive.

4. Locomotive strategy for the optimized rocker-bogie mechanism

In the previous section, the link parameters of rocker-bogie mechanism are optimized via the Taguchi method, which guarantees the stable behavior of mobile robot during climbing the stair as well as the excellent adaptability to various types of the stairs frequently encountered in indoor applications. In this section, the most suitable locomotive strategy for the proposed rocker-bogie mechanism is derived by kinetically analyzing its stair-climbing motion. To this end, a simplified mathematical model for the proposed rocker-bogie mechanism is built under the assumption that the rocker-bogie mechanism is in the quasi-static condition, that is, it moves at a sufficiently slow and constant velocity. Based on its stair-climbing motion classified into several phases according to the interaction between the wheels and the stair, the appropriate locomotive strategy is then developed. The effectiveness of the proposed locomotive strategy is subsequently examined and validated through the extensive simulations for different sizes of the stairs.

4.1. Mathematical modeling

Fig. 13 shows the schematic diagram of the proposed rocker-bogie mechanism interacting with the ground, where the traction/normal forces and the contact angle at each wheel are denoted by T_i, N_i and γ_i, $i=1, 2, 3$, respectively. M_b corresponds to the moment on the CM of the proposed rocker-bogie mechanism, which is primarily required to maintain the posture of its main body horizontally. The angles between two links l_2, l_3 and the horizontal axis x are denoted by θ_1 and θ_2, respectively and the angle between two links l_2 and l_4 is denoted by δ. For the simplicity of analysis, the mass of each link is assumed to be negligible compared to those of the wheels and the robot body, which are denoted by m_i, $i=1, 2, 3$ and m_b, respectively. Recall that

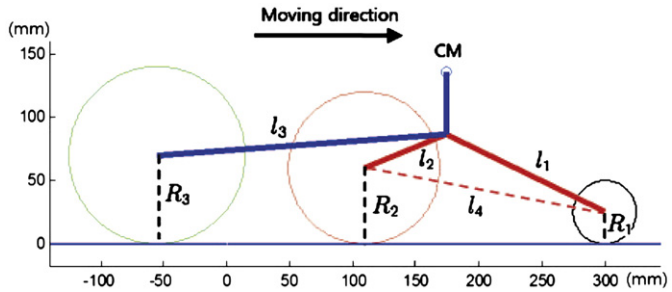

Fig. 11. Schematic diagram of the optimized rocker-bogie mechanism.

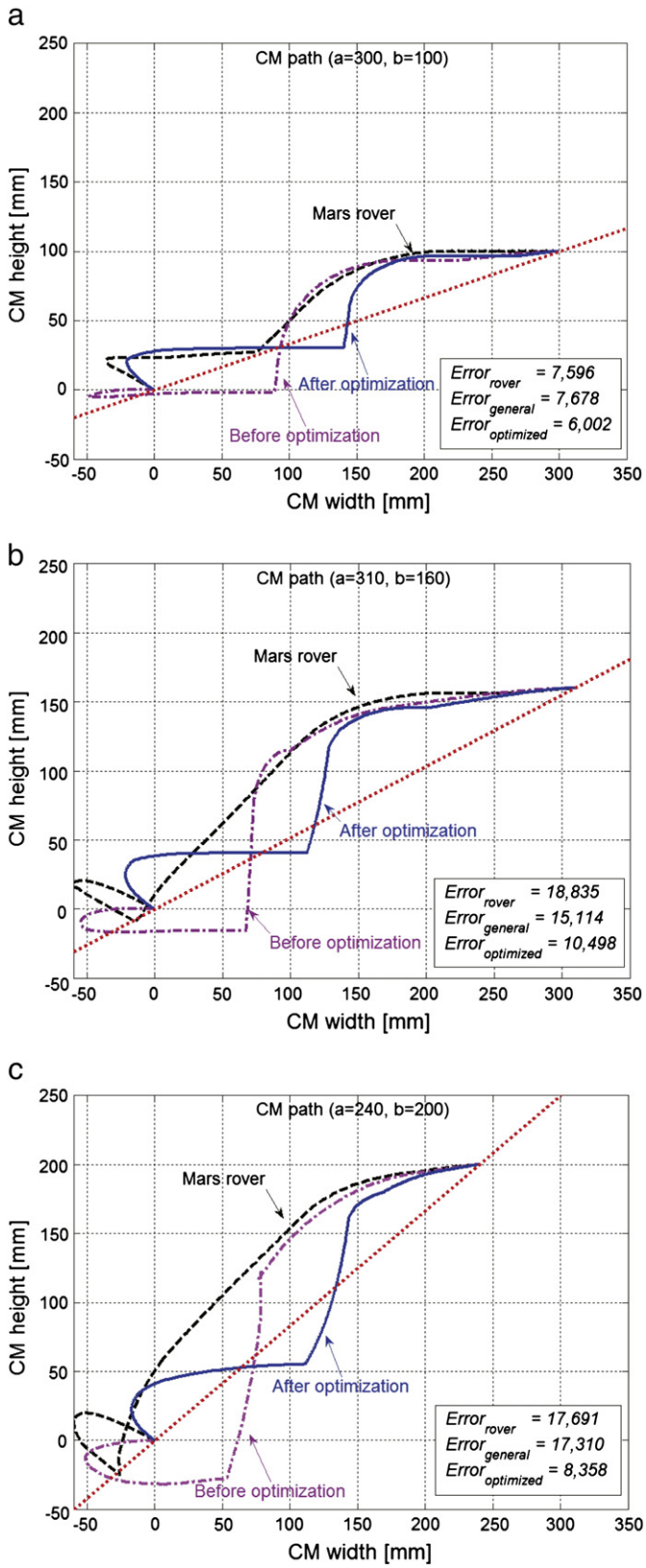

Fig. 12. Comparison of the CM trajectories of the optimized/general rocker-bogie mechanisms and Mars rover Spirit.

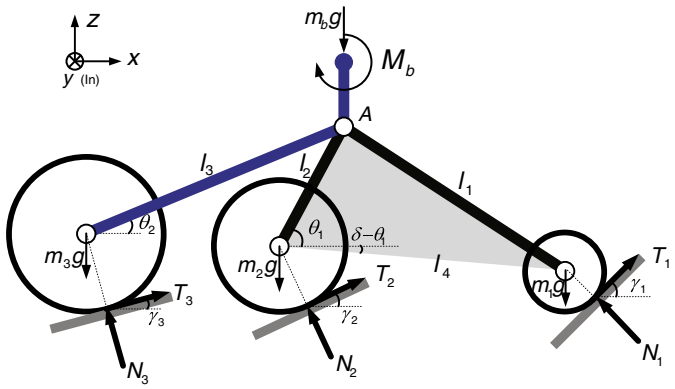

Fig. 13. Schematic diagram of the proposed rocker-bogie mechanism interacting with the ground.

although the analysis in this section is carried out under the assumption that the proposed rocker-bogie mechanism is in the quasi-static condition, this simplest model in Fig. 13 still allows capturing of the key concept of the locomotive strategy in Section 4.3.

Under the quasi-static condition, the resulting forces on the joint A of the bogie mechanism must be zero along the x- and z-axes so that the following equations are derived from the free body diagram shown in Fig. 14.

$$\begin{cases} A_x + \sum_{i=1}^{2}(T_i \cos\gamma_i - N_i \sin\gamma_i) = 0 \\ A_z + \sum_{i=1}^{2}(T_i \sin\gamma_i + N_i \cos\gamma_i - m_i g) = 0 \end{cases} \tag{7}$$

where A_x and A_z correspond to the reaction forces against the rocker mechanism. Similarly, the resulting moment $M_{bogie,A}$ on the joint A through the bogie mechanism along the y-axis also must be zero, which is derived as follows.

$$\begin{aligned} M_{bogie,A} = {} & (T_2 \sin\gamma_2 + N_2 \cos\gamma_2 - m_2 g) \times l_2 \cos\theta_1 \\ & -(T_1 \cos\gamma_1 - N_1 \sin\gamma_1) \times (l_4 \sin(\delta-\theta_1) + l_2 \sin\theta_1) \\ & -(T_1 \sin\gamma_1 + N_1 \cos\gamma_1 - m_1 g) \times (l_4 \cos(\delta-\theta_1) - l_2 cos\theta_1) \\ & -(T_2 \cos\gamma_2 - N_2 \sin\gamma_2) \times l_2 \sin\theta_1 = 0. \end{aligned} \tag{8}$$

Similarly, the resulting forces on the joint A of the rocker mechanism must be zero along the x- and z-axes so that the following equations are derived from the free body diagram shown in Fig. 15.

$$\begin{cases} -A_x + T_3 \cos\gamma_3 - N_3 \sin\gamma_3 = 0 \\ -A_z + T_3 \sin\gamma_3 + N_3 \cos\gamma_3 - (m_3 + m_b)g = 0. \end{cases} \tag{9}$$

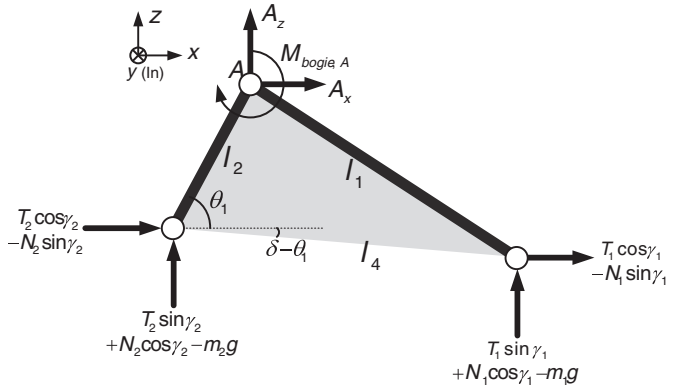

Fig. 14. Free body diagram of bogie mechanism.

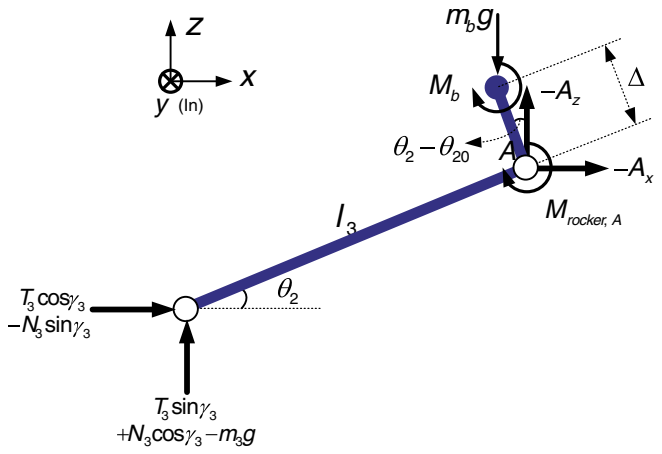

Fig. 15. Free body diagram of rocker mechanism.

The resulting moment $M_{rocker,A}$ acting on the joint A through the rocker mechanism along the y-axis also must be zero, which is given by

$$\begin{aligned} M_{rocker,A} = {} & (T_3\sin\gamma_3 + N_3\cos\gamma_3 - m_3 g)\times l_3\cos\theta_2 \\ & -(T_3\cos\gamma_3 - N_3\sin\gamma_3)\times l_3\sin\theta_2 \\ & -m_b g\times\Delta\sin(\theta_2-\theta_{20}) + M_b \end{aligned} \tag{10}$$

where θ_{20} corresponds to the value of original θ_2 when the proposed rocker-bogie mechanism is on an even terrain. According to the geometric relation between wheels and links on the even terrain shown in Fig. 11, it is obtained by

$$\theta_{20} = atan2\left(\left(A_{0,2}-W_{30,2}\right),\left(A_{0,1}-W_{30,1}\right)\right) \tag{11}$$

where $A_{0,i}$ and $W_{*,i}$, $i=1,2$ denote the ith elements of A_0 and W_*, respectively, which are given by

$$\begin{cases} W_{10} = \begin{bmatrix} 0 \\ R_1 \end{bmatrix}, W_{20} = \begin{bmatrix} -\sqrt{l_4^2-(R_1-R_2)^2} \\ R_2 \end{bmatrix} \\ A_0 = \dfrac{l_2}{l_4}\begin{bmatrix} \cos\delta & -\sin\delta \\ \sin\delta & \cos\delta \end{bmatrix}(W_{10}-W_{20}) + W_{20}, \\ W_{30} = \begin{bmatrix} A_{0,1}-\sqrt{l_3^2-\left(A_{0,2}-R_3\right)^2} \\ R_3 \end{bmatrix}, \end{cases} \tag{12}$$

Since the bogie and the rocker mechanisms are connected at the joint A, the following force equations are derived by combining Eq. (7) with Eq. (9) and should be satisfied regardless of whether the proposed rocker-bogie mechanism moves or not.

$$\begin{cases} \displaystyle\sum_{i=1}^{3}(N_i\cos\gamma_i - T_i\sin\gamma_i) = 0 \\ \displaystyle\sum_{i=1}^{3}(N_i\sin\gamma_i + T_i\cos\gamma_i - m_i g) - m_b g = 0. \end{cases} \tag{13}$$

It is worthwhile to note that there exist the reaction torques in real situations where at least one wheel stays on the riser of the stair, because the wheel torques are required to maintain the equilibrium configuration of the rocker-bogie mechanism. Please recall that in the quasi-static motion, the reaction torques can be ignored because the result of the quasi-static analysis describes the performance of the pure mechanical structure without any controller so that the resistance to movement such as the reaction torque can be handled as a type of disturbance and be canceled with an appropriate control method [29]. Furthermore, since the main thrust of this section is to derive a suitable locomotive strategy for the proposed rocker-bogie mechanism not by constructing a complicated model for the proposed mechanism but by capturing a key concept of its motions during climbing the stair, the reaction torques are not considered as in [16,23,24,29].

4.2. Friction requirement metric as performance measure

Among other measures evaluating the climbing capability of the mobile robot, the friction requirement metric μ_{req} is widely adopted, which is defined as the minimum friction coefficient required to climb the obstacles without slip [24,29]. For small μ_{req}, the mobile robot is less likely to start slipping during climbing the stair.

According to Coulomb's friction law, slip on the ith wheel may be avoided if the following condition is satisfied

$$T_i \le \mu \cdot N_i \tag{14}$$

where μ is a friction coefficient determined mainly by the materials of the wheel and the ground and, T_i and N_i correspond to the traction and normal forces of the ith wheel, respectively. However, since it is quite difficult to obtain an exact value of μ in real applications, a virtual friction coefficient μ_i^* for the ith wheel is introduced to examine the risk of slip [24], which is defined as

$$\mu_i^* = \frac{T_i}{N_i} = \frac{\tau_i / R_i}{N_i}$$

where τ_i and R_i denote the motor torque of the ith, wheel and its radius, respectively. If μ_i^* is smaller than μ, Eq. (14) is satisfied so that slip does not occur. Therefore, it is highly desirable to minimize μ_i^* in order to reduce the risk of slip. It is worthwhile to note that while the normal force N_i depends on the status of the mobile robot such as its posture, the motor torque τ_i can be arbitrarily selected due to kinematic redundancy of the mobile robot so that μ_i^* may be minimized by choosing the motor torques appropriately. According to [24,30], the friction requirement metric μ_{req} can be obtained by solving the following optimization problem

$$\max_n \left\{ \min_i (\mu_i^* - \overline{\mu})^2 \right\} \tag{15}$$

where $\overline{\mu}$ is the mean of all μ_i^*, i and n denote the number of wheels and the number of total simulation steps, respectively.

As a benchmark test, the friction requirement metric μ_{req} for the proposed rocker-bogie mechanism is calculated under the quasi-static condition shown in Eqs. (8), (10) and (13). In order to guarantee the strong contact between the wheels and the ground, it is also assumed that $N_i \ge 0$, $i = 1, 2, 3$. During the simulation, the proposed rocker-bogie mechanism is supposed to climb one step of the types I, II and III stairs in Fig. 3 and its step-climbing motion is divided into 8 phases according to the interaction between the wheels and the step. An exemplary snapshot of its climbing motion for the one step of the type I stair is shown in Fig. 16. Please note that the front, middle and rear wheels climb up the step during the phases 1, 4 and 7, respectively as confirmed in Fig. 16, which indicates that those phases will play kinetically dominant roles in determining the climbing capability of the proposed rocker-bogie mechanism.

Fig. 17 shows the friction requirement metrics under the quasi-static condition for one step of the types I, II and III stairs, which are denoted by the dotted, dash–dotted and solid lines, respectively. As shown in Fig. 17, there exist two kinds of peaks in the friction requirement metric. While the first peak occurs when the front wheel begins to move up along the riser of the step irrespective of the type of the stair, the second one happens depending on the type of the stair: for the type I stair, the second peak happens under same condition as in

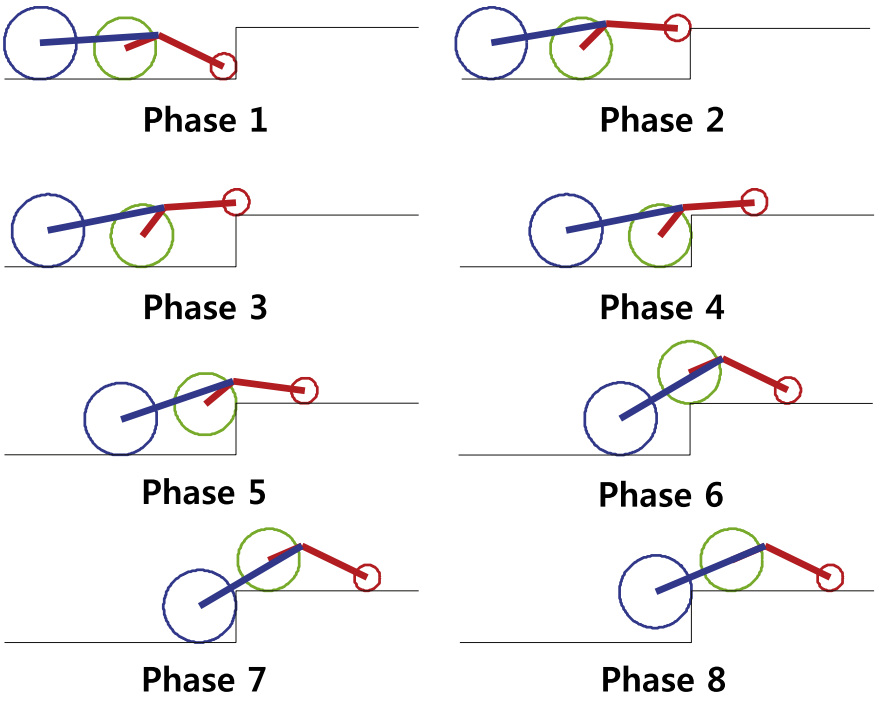

Fig. 16. Snapshot of step-climbing motion for the type I stair.

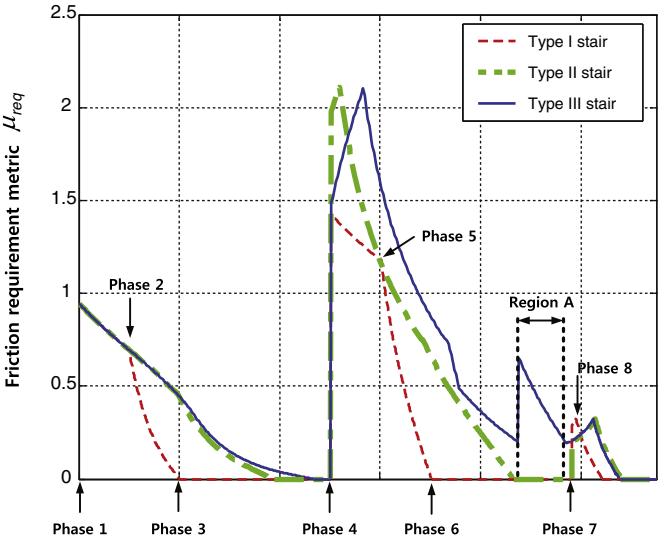

Fig. 17. Comparison of friction requirement metrics to climb one step of three stairs in Fig. 3 under the quasi-static condition.

the first one but for the types II and III stairs, the second peaks happen when the middle wheel rolls over the edge of the step after reaching its vertical end. Compared to the cases of the types I and II stairs, an additional peak is observed in the case of the type III stair, which is denoted by "region A" in Fig. 17. It is because the rear wheel begins to climb the riser of the step before the middle wheel finishes rolling over the edge of the step but the corresponding friction requirement metric is relatively smaller than those observed when the front and middle wheels start to climb the step. The maximum value ($=2.1$) of the friction requirement metric occurs when the middle wheel rolls over the edge of the step for the types II and III stairs. Even though the detailed dimensions of the proposed rocker-bogie mechanism are quite different and its front wheel size is too smaller than those in [24,29], the friction requirement metric seems too high in comparison with previous simulation results so that it is likely to suffer from undesirable slip and as a result, fail to climb the stair.

4.3. Improvement of climbing capability via kinetic analysis

It is worthwhile to note that the movements of the proposed rocker-bogie mechanism shown in Fig. 16 are not the results of the computed forces and torques because the proposed rocker-bogie mechanism is in the quasi-static condition. In fact, during the simulation, the mobile robot is placed at every successive position from the beginning to the end of the step and then, the state of quasi-static equilibrium is calculated so that each simulation step is independent from one another. [29]. Therefore, for a sufficiently small simulation step, dynamical effects such as acceleration for the robot body or angular acceleration for the wheel can be neglected at each simulation step. Based on this additional assumption, the kinetics of the proposed rocker-bogie mechanism is tactfully exploited to build a suitable locomotive strategy for the proposed rocker-bogie mechanism, which is concerned with the relation between the motion of the mobile robot and its causes, namely forces and torques. Contrary to the previous analysis focusing on keeping the quasi-static equilibrium of the proposed rocker-bogie mechanism around the joint A, the moment on each wheel is considered to escape from the situation where the mobile robot cannot climb the stair and halts where it is because of slip [23].

The resulting moments M_{bogie,W_1}, M_{bogie,W_2} and M_{rocker,W_3} acting on the front, middle and rear wheels through the bogie and the rocker mechanisms along the y-axis are derived from the free body diagrams in Figs. 14 and 15, respectively as follows:

$$\begin{aligned} M_{bogie,W_1} &= (T_2\sin\gamma_2 + N_2\cos\gamma_2 - m_2 g)\times l_4\cos(\delta-\theta_1) \\ &\quad +(T_2\cos\gamma_2 - N_2\sin\gamma_2)\times l_4\sin(\delta-\theta_1) \\ &\quad +A_x\times(l_4\sin(\delta-\theta_1)+l_2\sin\theta_1) \\ &\quad +A_z\times(l_4\cos(\delta-\theta_1)-l_2\cos\theta_1) \end{aligned} \tag{16}$$

$$\begin{aligned} M_{bogie,W_2} &= A_x\times l_2\sin\theta_1 - A_z\times l_2\cos\theta_1 \\ &\quad -(T_1\cos\gamma_1 - N_1\sin\gamma_1)\times l_4\sin(\delta-\theta_1) \\ &\quad -(T_1\sin\gamma_1 + N_1\cos\gamma_1 - m_1 g)\times l_4\cos(\delta-\theta_1) \end{aligned} \tag{17}$$

$$\begin{aligned} M_{rocker,W_3} &= m_b g\times(l_3\cos\theta_2 - \Delta\sin(\theta_2-\theta_{20})) + M_b \\ &\quad -A_x\times l_3\sin\theta_2 + A_z\times l_3\cos\theta_2 \end{aligned} \tag{18}$$

where A_x and A_z are the resulting forces on the joint A along the x- and z-axes as described in Eqs. (7) and (9), respectively. Recall that the dominant peaks of the friction requirement metric occur while the front wheel climbs the step and the middle wheel rolls over the

edge of the step as shown in Fig. 17. Therefore, it is necessary to derive appropriate conditions based on the kinetic analysis which can reflect the states of the proposed rocker-bogie mechanism interacting with the ground specially during the phases 1–2 and 4–5.

In order for the front wheel to efficiently climb the step during the phase 1, M_{bogie,W_2} in Eq. (17) must be negative until the vertical position of the front wheel center becomes equal to that of the middle one, that is, $\delta=\theta_1$. After passing through that point, M_{bogie,W_2} is changed to positive until the front wheel finishes rolling over the edge of the step, which serves not only to guarantee the strong contact with the ground but also to prevent such instability as a tip-over of the proposed rocker-bogie mechanism. For the phase 4 where the middle wheel begins to climb the step, M_{bogie,W_1} in Eq. (16) must be negative and M_{rocker,W_3} in Eq. (18) must be positive in order to efficiently lift up the middle wheel. For the phase 5 where the middle wheel starts to roll over the edge of the step, M_{bogie,W_2} is again set to positive and will be kept until completing climbing the step. Except for the phase 4 where $M_{rocker,W_3}>0$ is applied to lift up the middle wheel, $M_{rocker,A}$ is set to zero for other phases. For all phases, $N_i\geq 0$, $i=1,2,3$ is also assumed to ensure good contact with the ground. The detailed kinetic conditions are depicted in Fig. 18 for the type I stair, which can be similarly applied to the types II and III stairs.

From the viewpoint of the kinetic analysis of the stair-climbing motion, the optimization problem to obtain the friction requirement metric μ_{req} can be summarized as follows:

$$\max_n\left\{\min_i\left(\mu_i^*-\bar{\mu}\right)^2\right\} \tag{19}$$

$$\text{subject to}\begin{cases}\sum_{i=1}^{3}\left(N_i\cos\gamma_i-T_i\sin\gamma_i\right)=0\\ \sum_{i=1}^{3}\left(N_i\sin\gamma_i+T_i\cos\gamma_i-m_ig\right)-m_bg=0 N_i\geq 0\quad i=1,2,3\\ \begin{cases}M_{bogie,W_2}<0,\\ M_{rocker,A}=0\end{cases}\text{if }\ \delta-\theta_1<0\ \text{ for phase }\ 1\\ \begin{cases}M_{bogie,W_2}>0,\\ M_{rocker,A}=0\end{cases}\text{if }\ \delta-\theta_1\geq 0\ \text{ for phase }\ 1\\ \begin{cases}M_{bogie,W_1}>0,\\ M_{rocker,W_3}<0\end{cases}\text{for phase }\ 4\\ \begin{cases}M_{bogie,W_2}>0,\\ M_{rocker,A}=0\end{cases}\text{for other phases.}\end{cases}$$

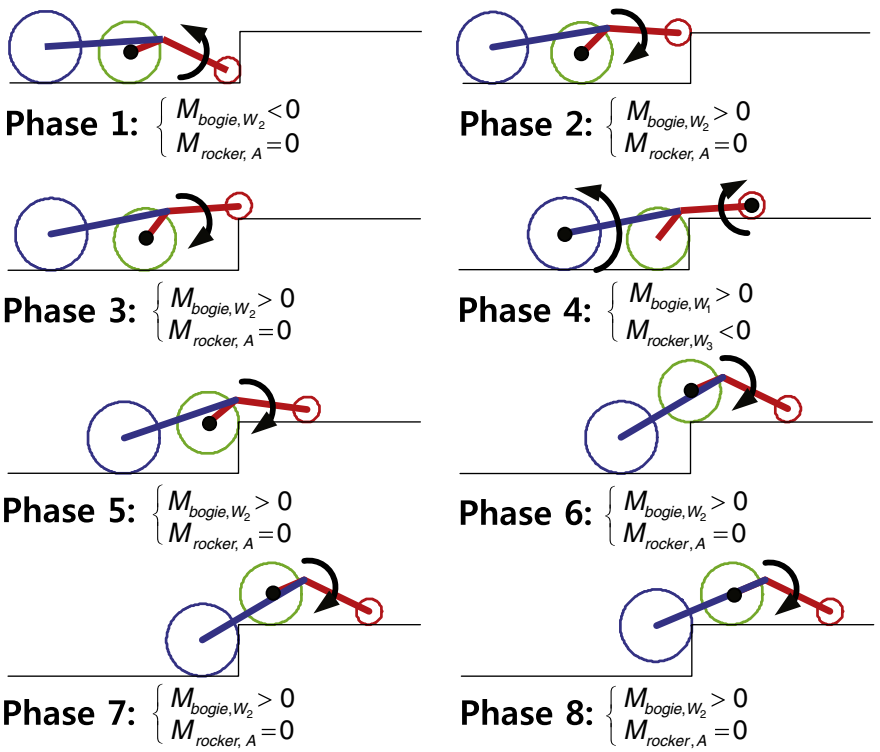

Fig. 18. Kinetic conditions with respect to each climbing phase for the type I stair.

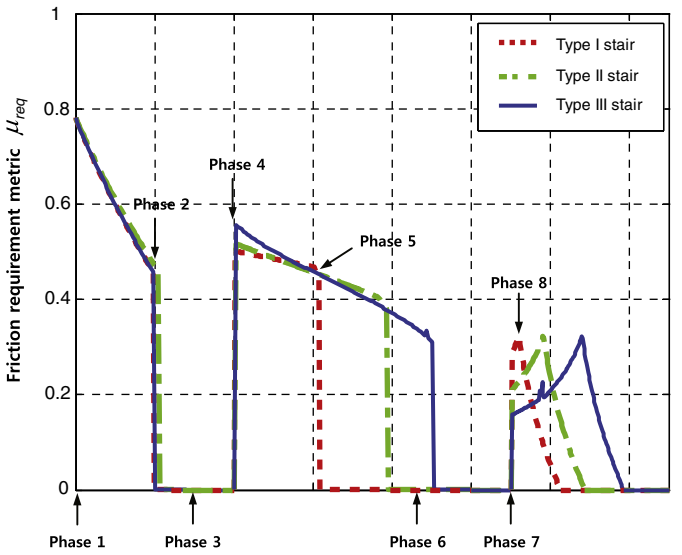

Fig. 19. Comparison of friction required metrics from kinetic analysis to climb one step of three stairs in Fig. 3.

Fig. 19 shows the friction requirement metrics obtained from the kinetic analysis, where the dotted, dash–dotted and solid lines denote the cases of climbing the step of the types I, II and III stairs, respectively. Compared to those in Fig. 17, the maximum values of the friction requirement metrics are reduced from 0.94 to 0.78 when the front wheel starts to climb the step of all type stairs and from 2.1 to 0.59 when the middle wheel begins to climb the step of type III stair, respectively. Recall that both results shown in Figs. 17 and 19 evaluate the climbing capability of the proposed rocker-bogie mechanism in view of the mechanical structure without any control strategy [24]. Therefore, compared to the case that only the effect of M_{bogie,W_2} is considered, the resulting friction requirement metric corresponding to the case that both effects of M_{bogie,W_1} and M_{rocker,W_3} are simultaneously considered are significantly improved, which can explain why the second peak of the friction requirement metric shown in Fig. 17 disappears in Fig. 19. Combined with an appropriate control methodology, the proposed locomotive strategy based on the kinetic analysis enables the optimized rocker-bogie mechanism to efficiently climb the various types of the stairs without deteriorating its stable behavior.

5. Conclusion

The link parameters of the rocker-bogie mechanism are optimized via the well-known Taguchi method to improve its climbing capability as well as adaptability for various types of the stairs. In order to guarantee the stable behavior of the proposed rocker-bogie mechanism during climbing the stair, the area between the trajectory of its CM and the straight line whose slope is determined by the stair is minimized by the Taguchi method under kinematic constraints to prevent the interferences between the mobile robot and the ground. As a result, the CM trajectory of the optimized rocker-bogie mechanism becomes close to the straight line compared to general rocker-bogie mechanism and Mars rover Spirit and also, the shortcoming of the general rocker-bogie mechanism such as undesired backward movement is considerably reduced, which implies that the proposed rocker-bogie mechanism enables climbing of the stair more rapidly and efficiently. As a criterion to evaluate the climbing performance of the proposed rocker-bogie mechanism, the friction requirement metric is chosen. A suitable locomotive strategy such as the motor torques to prevent slip is derived based on the kinetic analysis to reflect the states of the proposed rocker-bogie mechanism interacting with the ground. Through extensive simulations, it is verified that the suggested locomotive strategy from the kinetic analysis makes the proposed rocker-bogie mechanism less susceptible to slip so that it can climb the step more efficiently.

Acknowledgment

This work was supported in part by the National Research Foundation of Korea (NRF) grant funded by the Korea government (MEST) (No. 2009-0087640) and in part by the second stage of the Brain Korea 21 Program of Seoul National University.

References

[1] S. Fish, UGV's in future combat systems, Proceedings of the SPIE-unmanned Ground Vehicle Technology VI, Orlando, USA, 2004, pp. 288–291.
[2] F.L. Menn, P. Bidaud, F.B. Amar, Generic differential kinematic modeling of articulated multi-monocycle mobile robots, Proceedings of the 2006 IEEE International Conference on Robotics and Automation, Orlando, USA, 2006.
[3] A. Halme, I. Leppanen, J. Soumela, S. Ylonen, I. Kettunen, Workpartner: interactive human-like service robot for outdoor applications, International Journal of Robotics Research 22 (2003) 627–640.
[4] C. Distante, G. Indivery, G. Reina, An application of mobile robotics for olfactory monitoring of hazardous industrial sites, Industrial Robot: An International Journal 36 (2009) 51–59.

[5] R. Volpe, J. Balaram, T. Ohm, R. Ivlev, Rocky7: a next generation Mars rover prototype, Advanced Robotics 11 (1997) 341–358.
[6] R.A. Lindemann, C.J. Voorhees, Mars exploration rover mobility assembly design, test and performance, IEEE International Conference on Systems, Man and Cybernetics, Waikoloa, USA, 2005.
[7] J. Erickson, Living the dream: an overview of the mars exploration project, IEEE Transactions on Robotics and Automation 13 (2006) 12–18.
[8] B. Chen, R. Wang, Y. Jia, L. Guo, L. Yang, Design of a high performance suspension for lunar rover based on evolution, Acta Astronautica 64 (2009) 925–934.
[9] A. Mechdari, H.N. Pishkenari, A.L. Gaskarimahalle, S.H. Mahboobi, R. Karimi, A novel approach for optimal design of a rover mechanism, Journal of Intelligent and Robotic Systems 44 (2005) 291–312.
[10] K. Nagatani, A. Yamasaki, K. Yoshida, T. Adachi, Development and control method of six-wheel robot with rocker structure, Proceedings of the 2007 IEEE International Workshop on Safety, Security and Rescue Robotics, Rome, Italy, 2007.
[11] W. Chung, G. Kim, M. Kim, Development of the multi-functional indoor service robot PSR systems, Autonomous Robotics 22 (2007) 1–17.
[12] M. Wada, M. Wada, Mechanism and control of a 4WD robotic platform for omnidirectional wheelchairs, Proceedings of the 2009 IEEE/RSJ International Conference on Intelligent Robots and Systems, St. Louis, USA, 2009.
[13] F. Michaud, et al., Multi-modal locomotion robotic platform using leg-track-wheel articulations, Autonomous Robots 18 (2005) 137–156.
[14] D. Chugo, K. Kawabata, H. Kaetsu, H. Asama, T. Mishima, Step climbing omnidirectional mobile robot with passive linkages, Proceedings of SPIE-optomechatronic Systems Control, Sapporo, Japan, 2005.
[15] S. Nakajima, Development of four-wheel-type mobile robot for rough terrain and verification of its fundamental capability of moving on rough terrain, Proceedings of IEEE International Conference on Robotics and Biomimetics, Bangkok, Thailand, 2009.
[16] R. Siegwart, P. Lamon, T. Estier, M. Lauria, R. Piguet, Innovative design for wheeled locomotion in rough terrain, Robotics and Autonomous Systems 20 (2002) 151–162.
[17] S. Nakajima, Concept of a novel four-wheel-type mobile robot for rough terrain, RT-mover, Proceedings of IEEE International Conference on Intelligent Robots and Systems, St. Louis, USA, 2009.
[18] K. Six, A. Kecskem'ethy, Steering properties of a combined wheeled and legged striding excavator, Proceedings of the 10th World Congress on the Theory of Machines and Mechanisms, Oulu, Finland, 1999.
[19] M. Lacagnina, G. Muscato, R. Sinatra, Kinematics, dynamics and control of a hybrid robot wheeleg, Robotics and Autonomous Systems 45 (2003) 161–180.
[20] S. Li, H. Gao, Z. Deng, S. Li, H. Gao, Z. Deng, Mobility Performance Evaluation of Lunar Rover and Optimization of Rocker-Bogie Suspension Parameters, The 2nd international symposium on systems and control in aerospace and astronautics, Shenzhen, China, 2008.
[21] B.D. Harrington, C. Voorhees, The challenges of designing the rocker-bogie suspension for the mars exploration rover, Proceedings of the 37th Aerospace Mechanisms Symposium, 2004.
[22] M. Sato, A. Kanda, K. Ishii, Simultaneous optimization of a wheeled mobile robot structure and a control parameter, 5th International Workshop on Computational Intelligence and Applications, Hiroshima, Japan, 2009.
[23] C. Woo, H. Chli, S. Yoon, S. Kim, Y. Kwak, Optimal design of a new wheeled mobile robot based on a kinetic analysis of the stair climbing states, Journal of Intelligent and Robotic Systems 49 (2007) 325–354.
[24] T. Thueer, R. Siegwart, Mobility evaluation of wheeled all-terrain robots, Robotics and Autonomous Systems 58 (2010) 508–519.
[25] B.K. Rout, R.K. Mittal, Parametric design optimization of 2-DOF R–R planar manipulator—a design of experiment approach, Robotics and Computer-Integrated Manufacturing 24 (2008) 239–248.
[26] H. Kim, D. Kim, H. Yang, K. Lee, K. Seo, D. Chang, J. Kim, Development of a wall-climbing robot using a tracked wheel mechanism, Journal of Mechanical Science and Technology 22 (2008) 1490–1498.
[27] K. Lee, J. Kim, Controller gain tuning of a simultaneous multi-axis PID control system using the Taguchi method, Control Engineering Practice 8 (2000) 949–958.
[28] G.S. Peace, Taguchi Methods: Hands-on Approach, Addison-Wesley, New York, 1993.
[29] T. Thueer, A. Krebs, R. Siegwart, Performance comparison of rough-terrain robots—simulation and hardware, Journal of Field Robotics 24 (2007) 251–271.
[30] P. Lamon, A. Krebs, M. Lauria, R. Siegwart, S. Shooter, Wheel torque control for a rough terrain rover, Proceedings of IEEE International Conference on Robotics and Automation, New Orieans, USA, 2004.